Journal of Molecular Catalysis A: Chemical 350 (2011) 1–8

Contents lists available at SciVerse ScienceDirect

Journal of Molecular Catalysis A: Chemical

journal homepage: www.elsevier.com/locate/molcata

Editor's choice paper

Preparation of [Fe]-SSZ-24 through the isomorphous substitution of [B]-SSZ-24 with iron, and its catalytic properties in the isopropylation of biphenyl

Hiroaki Kawagoe[a], Kenichi Komura[a], Jong-Ho Kim[b], Gon Seo[b], Yoshihiro Sugi[a,*]

[a] Department of Material Science and Technology, Faculty of Engineering, Gifu University, Gifu 501-1193, Japan
[b] School of Applied Chemical Engineering, Chonnam National University, Gwangju 500-757, Republic of Korea

ARTICLE INFO

Article history:
Received 23 July 2011
Received in revised form 30 August 2011
Accepted 30 August 2011
Available online 7 September 2011

Keywords:
SSZ-24
Isomorphous substitution
Isopropylation
Biphenyl
Shape-selective catalysis

ABSTRACT

[Fe]-SSZ-24, a ferrosilicate with AFI topology, was prepared through an isomorphous substitution of [B]-SSZ-24 with iron, and applied for the isopropylation of biphenyl (BP) to understand the mechanism of shape-selective catalysis. The substitution of [B]-SSZ-24 with an aqueous solution of a limited amount of $Fe(NO_3)_3{\cdot}6H_2O$ effectively gave [Fe]-SSZ-24, and its XRD gave clear patterns of AFI topology without the peaks assigned to Fe_2O_3. [Fe]-SSZ-24 exhibited enhanced catalytic activity for the isopropylation of BP. Shape-selective formation of 4,4′-diisopropylbiphenyl (4,4′-DIPB) occurred at moderate temperatures (250–300 °C); however, the decreases of the selectivity for 4,4′-DIPB occurred at high temperatures (325–350 °C). On the other hand, the selectivities for 4,4′-DIPB in encapsulated products remained almost constant (*ca* 75%), irrespective of the reaction temperature and the SiO_2/Fe_2O_3 ratios. The differences in the selectivities for 4,4′-DIPB between bulk and encapsulated products indicate that shape-selective formation of 4,4′-DIPB occurs in the [Fe]-SSZ-24 channels, and these channels prevent the isomerization of 4,4′-DIPB, even at 350 °C. These results suggest that the channels of SSZ-24 can discriminate 4,4′-DIPB from other possible DIPB isomers at their transition states although high reaction temperatures cause isomerization at external acid sites.

Large pore molecular sieves of AFI topology, [Fe]-SSZ-24, [Al]-SSZ-24, MgAPO-5, ZnAPO-5, and SAPO-5, gave similar levels of selectivities for 4,4′-DIPB in the isopropylation of BP. These results indicate that the framework of AFI topology primarily controls shape-selective formation of 4,4′-DIPB, although catalytic activities of the materials were dependent on acidic properties.

1. Introduction

Large pore molecular sieves (LPMS) including zeolites, metallosilicates, and metallophosphates are the most promising microporous crystals for achieving highly shape-selective catalysis because their pores are uniformly distributed and because they have dimensions that allow both organic reactants and products to enter, to be accommodated, and to leave [1–5]. Among them, LPMS with 12- and 14-membered ring (12- and 14-MR) entrances are expected for the catalysts of the alkylation of polynuclear aromatics [3–20]. For example, dealuminated H-mordenite (MOR) selectively gave 4,4′-diisopropylbiphenyl (4,4′-DIPB) in the isopropylation of biphenyl (BP) [3,5–8]. It has been of great interest to elucidate the catalytic features of the LPMS pores because confined circumstances of the materials highly influence shape-selective catalysis. Recently, we studied the alkylation of BP over various zeolites with one-dimensional 12-MR and 14-MR pore entrances and over three-dimensional zeolites with 12-MR pore entrances from the aspects of steric restriction at the transition states of the product isomers in the channels [9–17].

SSZ-24 is a high-silica LPMS isostructural with $AlPO_4$-5 (AFI topology) with 12-membered ring cylindrical channels and pore entrances of 0.72 nm radii [21]. Zones et al. first synthesized SSZ-24 in its pure-silica form using 1-trimethylammonioadamantane as a structure-directing agent (SDA) [22]. The borosilicate version ([B]-SSZ-24) was subsequently synthesized using a calcined form of boron-substituted zeolite β ([B]-BEA) as the boron and silicon sources [23]. Lobo and Davis also reported the synthesis of [B]-SSZ-24 using N(16)-methylasparteinium bromide $[MeSPA]^+Br^-$ as the SDA and sodium borate as the source of boron, and they converted to [Al]-SSZ-24 by an isomorphous substitution with aluminum nitrate [24]. More recently, we developed a new method of [Al]-SSZ-24 by phase transformation of zeolite β ([Al]-BEA) using $[MeSPA]^+OH^-$ as the SDA [25].

It is important to understand how the zeolite properties, such as structure of channels and acidity, influences shape-selective catalysis. In particular, we have been interested in the catalytic properties of isostructural LPMS with AFI topology in the isopropylation of BP,

* Corresponding author.
E-mail address: ysugi@gifu-u.ac.jp (Y. Sugi).

1381-1169/$ – see front matter © 2011 Elsevier B.V. All rights reserved.
doi:10.1016/j.molcata.2011.08.027

because they have slightly bigger pore entrances and channels compared to MOR. We have studied the isopropylation of BP over LPMS with AFI topology, [Al]-SSZ-24, MgAPO-5, ZnAPO-5, and SAPO-5, and discussed that the topology is a key factor in shape-selective formation of 4,4′-DIPB [18–20]. It is also important to elucidate the influences of acidic properties of zeolites on shape-selective catalysis. We consider that [Fe]-SSZ-24 is an appropriate candidate to study the influences of acidity on shape-selective catalysis in AFI channels, because [Fe]-SSZ-24 has AFI topology with weak acidity.

In this paper, we studied the preparation of [Fe]-SSZ-24 by an isomorphous substitution of [B]-SSZ-24 with iron, and applied it for the isopropylation of BP to elucidate the relation between the acidic and catalytic properties and to determine the role of topology and acidity in shape-selective catalysis through comparison to other isostructural LPMS with AFI topology.

2. Experimental

2.1. Synthesis of [Fe]-SSZ-24

[B]-SSZ-24 was synthesized by hydrothermal conditions using $[MeSPA]^+OH^-$ according to a procedure in the literature [23]. The typical gel composition is as follows SiO_2:$[MeSPA]^+OH^-$:NaOH:B_2O_3:H_2O = 1:0.2:0.1:0.04:50. SiO_2 (Carb-O-Sil M5) 0.608 g, $[MeSPA]^+OH^-$ 2.9125 g, $Na_2B_4O_7{\cdot}10H_2O$ 0.0766 g, 32 wt.% NaOH solution 0.0791 g, water 6.5474 g, and [B]-BEA (SiO_2/B_2O_3 = 50) 0.0125 g as seeds were placed in Teflon container, and resultant gel was stirred during 3 h. Then, the gel was transferred to Teflon-lined autoclave, heated at 175 °C during 6 d. After the crystallization was completed, the autoclave was cooled to room temperature. The obtained BEA zeolite was collected, washed thoroughly with water, and dried overnight at room temperature. The resultant zeolites were heated in a flow of air (50 ml/min) with temperature programmed rate of 2 °C/min up to 650 °C, and calcined for 6 h under an air stream (50 ml/min). [B]-SSZ24 with 53.0 of SiO_2/B_2O_3 was obtained. [B]-SSZ-24 (1.0 g) was then deboronated by stirring with 100 ml of 0.01N hydrochloric acid for 1 d. Then, resulting [B]-SSZ-24 after calcination at 650 °C was converted to [Fe]-SSZ-24 according to analogous method for the transformation of [B]-SSZ-24 to [Al]-SSZ-24 [24]. [B]-SSZ-24 was heated at 80 °C with an aqueous $Fe(NO_3)_3$ solution (1:0.5:50 (weight ratio) [B]-SSZ-24:$Fe(NO_3)_3{\cdot}9H_2O$:H_2O) for 18 h with stirring. After cooling the mixture, the solid was filtered and washed two times with 0.5 mol/l hydrochloric acid. Then, the resultant sample was dried at 40 °C overnight and calcined at 550 °C for 6 h. The samples with n times repetitions of the substitution with $Fe(NO_3)_3$/[B]-SSZ-24 = 0.5 were abbreviated Fn (n = 1–5). Thus, F1, F3, and F5 were used as catalysts. The SiO_2/Fe_2O_3 ratios of F1, F3, and F5 were 55, 38, and 28, respectively.

Isomorphous substitution of [B]-SSZ-24 with the ratio of [B]-SSZ-24:$Fe(NO_3)_3{\cdot}9H_2O$:H_2O (1:2.0:50 weight) was also examined to know the influence of the co-precipitation of ferric hydroxide on the zeolite. The obtained solid was filtered and washed two times with water. Then, the resultant sample was dried at 40 °C overnight and was calcined at 550 °C for 6 h. The samples of the zeolites with $Fe(NO_3)_3$/[B]-SSZ-24 = 2.0 were abbreviated Cn (n = 1–5).

The textual properties of [Fe]-SSZ-24 prepared by isomorphous substitution of [B]-SSZ-24 are summarized in Table 1.

Table 1
Textural properties of [Fe]-SSZ-24 zeolites.

	SiO_2/B_2O_3	SiO_2/Fe_2O_3	Surface area (m^2/g)	Pore volume (cm^3/g)
Calcined	53	–	379	0.16
Deboronated	361	–	343	0.14
F1	–	53	421	0.21
F3	–	38	261	0.10
F5	–	28	191	0.067
C3	–	6.5	380	0.15
C5	–	3.1	327	0.14

2.2. Isopropylation of BP

The isopropylation of BP was carried out in a 100-ml SUS-316 autoclave under propene pressure. Typical reaction conditions were 3.9 g of biphenyl (25 mmol) and 0.125 g of the catalyst with 0.8 MPa propene pressure at 250–350 °C for 4 h. An autoclave containing BP and the catalyst was purged with nitrogen before heating. After reaching the reaction temperature, propene was introduced to the autoclave, and the reaction was started by agitation. The pressure was kept constant throughout the reaction. After cooling the autoclave and release of excess propene, the catalysts were filtered off, and the bulk products were diluted with toluene. The products were analyzed by a Gas Chromatograph (GC-14C or GC-18A, Shimadzu Corporation, Kyoto, Japan) equipped with an Ultra-1 capillary column (25 m × 0.2 mm, 0.25 μm thickness, Agilent Technologies, MA, U.S.A.) and confirmed by a Shimadzu Gas Chromatograph-Mass Spectrometer (GC-MS-5000) using the same type column.

The yield of each product was calculated on the basis of the amount of starting BP, and the selectivities for each isopropylbiphenyl (IPBP) and diisopropylbiphenyl (DIPB) isomers were expressed according to the total amounts of each IPBP and DIPB isomers, respectively.

The analysis of the encapsulated products in the catalyst used for the reaction was carried out as follows. The catalyst was filtered off, washed with 200 ml of acetone, and dried at 110 °C for 12 h. Then, 50 mg of the resultant catalyst was carefully dissolved in 3 ml of aqueous hydrofluoric acid (47%) at room temperature. This solution was basified with solid potassium carbonate, and was extracted three times with 20 ml of dichloromethane. After removing the solvent *in vacuo* from the collected organic phases, the residue was dissolved in 5 ml of toluene and was subjected to a GC analysis following the same procedure as for the bulk products.

2.3. Characterization of the zeolites

Crystal structures of the zeolite were determined by powder X-ray diffraction using a Shimadzu XRD-6000 with Cu Kα radiation (λ = 1.5418 Å). An elemental analysis was performed by inductive coupled plasma atomic emission spectroscopy on a JICP-PS-1000 UV (Leeman Labs Inc., CA, USA). Scanning electron microscopy (SEM) was recorded by using an S-4300 FE-SEM microscope (Hitachi Corporation, Tokyo, Japan). N_2 adsorption measurements were performed on a Belsorp 28SA (Bel Japan, Osaka, Japan). Ammonia-temperature programmed desorption (NH_3-TPD) was measured using a TPD-66 apparatus (Bell Japan). Here, the catalyst was evacuated at 400 °C for 1 h, and ammonia was adsorbed at 100 °C, followed by further evacuation for 1 h. Then, the sample was heated from 100 to 710 °C at a rate of 10 °C/min under a helium stream. A TG analysis was performed using a Shimadzu TG-DTG-50 analyzer with a temperature-programmed rate of 10 °C/min in an air stream. The adsorption of *o*-xylene was measured by a gravimetric method using a microbalance at 25 °C and after the evacuation of the sample at 500 °C.

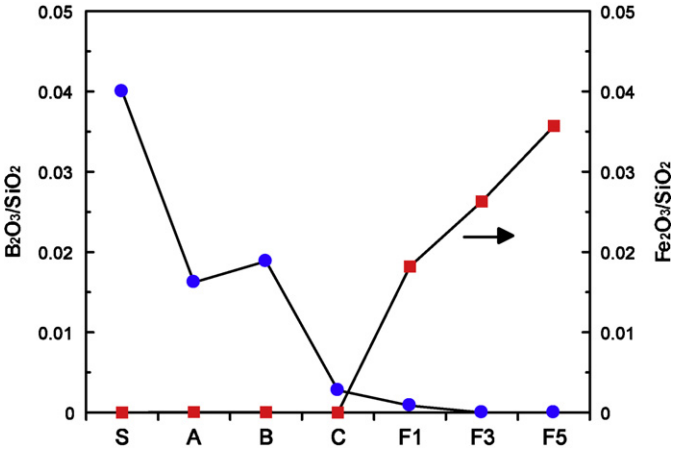

Fig. 1. Isomorphous substitution of [B]-SSZ-24 to [Fe]-SSZ-24. Substitution conditions: [B]-SSZ-24:$Fe(NO_3)_3{\cdot}9H_2O$:H_2O = 1:0.5:50 (weight ratio); temperature, 80 °C; and period, 18 h. Legends: S: starting gel; A: as-synthesized [B]-SSZ-24; B: calcined [B]-SSZ-24; C: deboronated [B]-SSZ-24; F1, F3, F5: sample of repetition times of substitution.

3. Results and discussion

3.1. Preparation and properties of [Fe]-SSZ-24

[B]-SSZ-24 (SiO_2/B_2O_3 = 53; B_2O_3/SiO_2 = 0.0377) was prepared under hydrothermal conditions by using $[MeSPA]^+OH^-$ as the SDA according to the methods in the literature [24]. [Fe]-SSZ-24 was then prepared from deboronated [B]-SSZ-24 by isomorphous substitution with ferric nitrate by the similar methods for [Al]-SSZ-24 [24].

It is important to choose the appropriate amount of aqueous solution of $Fe(NO_3)_3{\cdot}9H_2O$ for effective substitution on the framework of [B]-SSZ-24 to form [Fe]-SSZ-24 because the Fe^{3+} cations in the nitrate could be easily hydrolyzed to an ferric cluster, and precipitated as ferric hydroxide [26]. Fig. 1 shows the influence of the boron and iron contents on the substitution with $Fe(NO_3)_3{\cdot}9H_2O$/[B]-SSZ-24 = 0.5 (weight ratio). The boron content of [B]-SSZ-24 decreased rapidly by deboronation and substitution, and the SiO_2/Fe_2O_3 ratios for [Fe]-SSZ-24 were 55, 38, and 28 for F1, F3, and F5 samples, respectively. The color of these samples was pale off-white to yellow after calcination at 550 °C for 6 h. These results suggest that the substitution was accompanied by the precipitation of ferric hydroxide during the treatment of the ferric nitrate solution with [B]-SSZ-24. In other words, the incorporation of the Fe species with frameworks accompanies the formation of ferric hydroxide, independently from the substitution with zeolites. Actually, a large amount of Fe_2O_3 particles were found by SEM observation for calcined C3 samples substituted with $Fe(NO_3)_3{\cdot}9H_2O$/[B]-SSZ-24 = 2. Resultant C3 and C5 samples had much lower SiO_2/Fe_2O_3 ratios than F3 and F5 samples, as shown in Fig. S1 in Supporting Information. However, particle sizes of Fe_2O_3 cannot be estimated because the peaks due to them are too weak. These results mean that the precipitation of the ferric hydroxide, leading to Fe_2O_3 by calcination, occurred simultaneously during the substitution of [B]-SSZ-24 or the Fe incorporation into the voids of the frameworks formed by deboronation. These materials, C3 and C5, are brown in color after the calcination. The textural properties of the [Fe]-SSZ-24 prepared by isomorphous substitution are shown in Table 1.

Fig. 2 shows the XRD pattern of the calcined [Fe]-SSZ-24 samples. F1, F3, and F5 have almost the same patterns as the as-synthesized and calcined [B]-SSZ-24; however, the peaks of [Fe]-SSZ-24 for C3 and C5 were relatively small compared with those

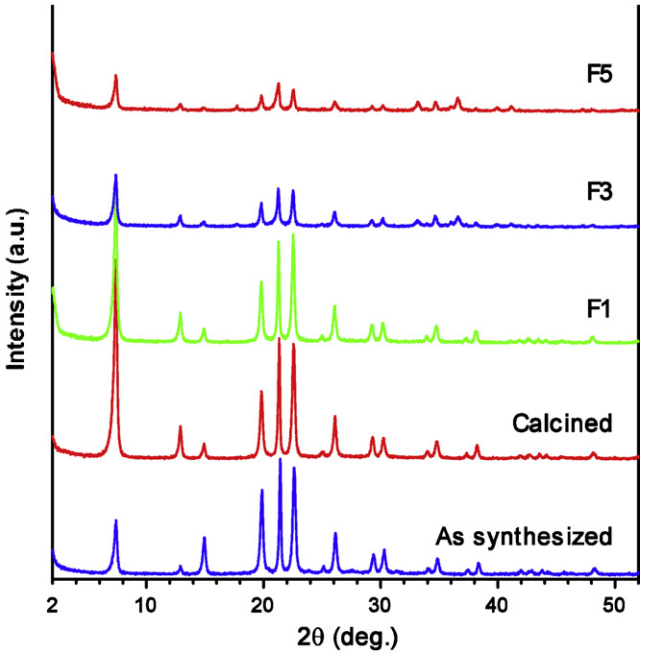

Fig. 2. XRD pattern of as-synthesized and calcined [B]-SSZ-24 and [Fe]-SSZ-24. Substitution conditions: F1, F3, and F5: [B]-SSZ-24:$Fe(NO_3)_3{\cdot}9H_2O$:H_2O = 1:0.5:50 (weight ratio). C3 and C5: [B]-SSZ-24:$Fe(NO_3)_3{\cdot}9H_2O$:H_2O = 1:2.0:50 (weight ratio). Temperature: 80 °C; period: 18 h.

of the original [B]-SSZ-24, and a new diffraction at around 36° appeared for C3 and C5. This weak diffraction is due to Fe_2O_3 with poor crystallinity [27], which results in no observation of the other peaks. These results also mean that an efficient substitution of B to Fe occurred by the substitution when the ratio of $Fe(NO_3)_3$/[B]-SSZ-24 was 0.5; however, severe precipitation of ferric hydroxide due to the hydrolysis of Fe^{3+} occurred at a ratio of 2.0 for $Fe(NO_3)_3$/SSZ-24. We must note that the deposition of ferric hydroxide and the resulting Fe_2O_3 formation probably occurred even for the substitution using small amounts of ferric nitrate by our method.

SEM images of [Fe]-SSZ-24 prepared by isomorphous substitution of [B]-SSZ-24 shown in Fig. 3 support the results discussed above. Clear crystal images were observed for F1 and F3; however, the crystals were accompanied by small particles in F5. Moreover, Fe_2O_3 particles were observed for C3; however, these Fe_2O_3 particles are almost amorphous judging from their XRD patterns.

Fig. 4 shows the N_2 adsorption isotherms of [Fe]-SSZ-24. F1 and F3 adsorbed large amounts of N_2 compared with the original [B]-SSZ-24; however, the further substitution in F5 was accompanied by a decrease in N_2 adsorption. On the other hand, N_2 adsorption on C3 and C5 decreased much more than that on [B]-SSZ-24. These results suggest that the site due to B species in F1 and F3 were substituted with ferric-cation without significant choking from the Fe_2O_3 particles. Unfortunately, the formation of the precipitate by repetitive substitution procedure eventually caused a choke of the channels of the zeolite. This result was clearly seen in C3 and C5 after the calcination. Thus, the substitution with the least formation of ferric hydroxide can be achieved by using an appropriate amount of the $Fe(NO_3)_3$ solution.

Fig. 5 shows the adsorption of *o*-xylene on [B]-SSZ-24 and [Fe]-SSZ-24 (F1 and F3). [B]-SSZ-24 and F3 rapidly adsorbed *o*-xylene, which is indicative of LPMS. The results mean that *o*-xylene can adsorb rapidly into the channels of F3 and [B]-SSZ-24, and that the channels of F3 are not choked severely by Fe_2O_3 due to cluster formation. On the other hands, the adsorption on C3 was less than that of F3 and [B]-SSZ-24. This decrease means that some of the pore entrances of C3 were choked or narrowed by Fe_2O_3 formation.

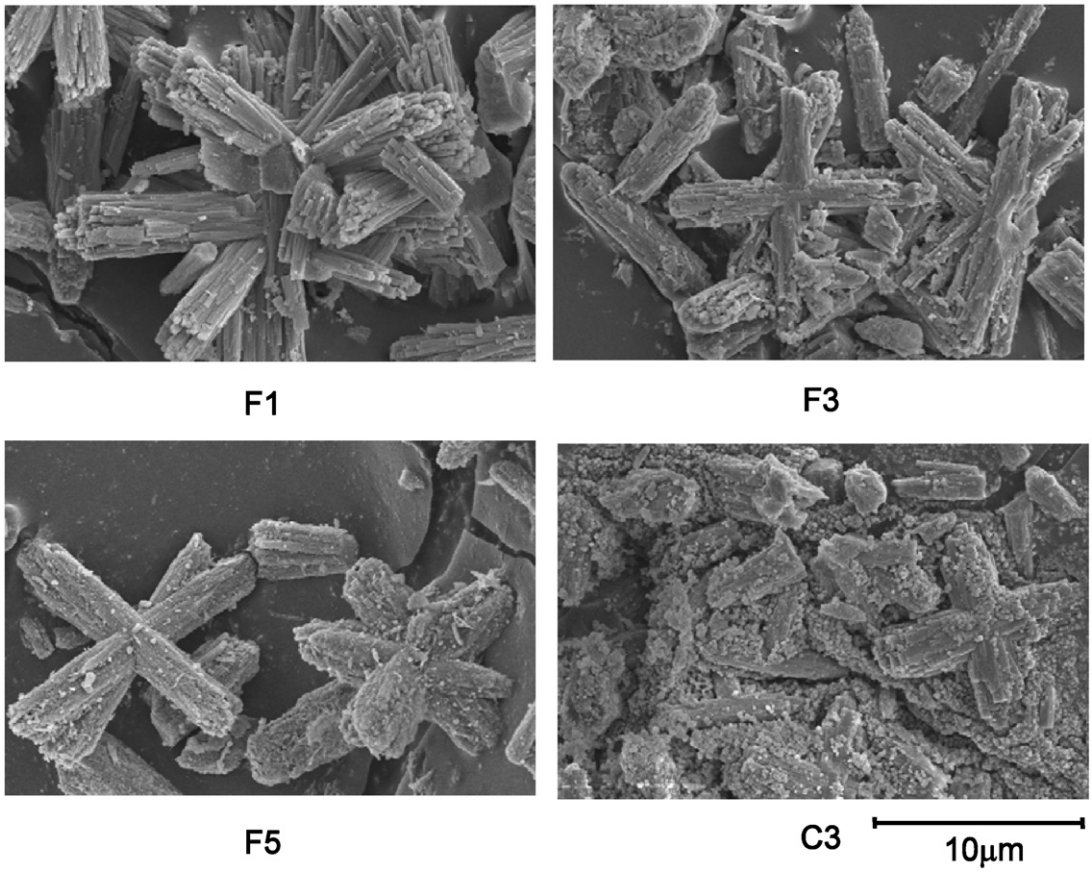

Fig. 3. SEM image of [Fe]-SSZ-24.

These results mean that the substitution of B to Fe is not a rapid process compared with the precipitation of ferric hydroxide at the surface of the extra-framework by the hydrolysis of the ferric cations.

NH_3-TPD was measured to know the acidity of [Fe]-SSZ-24. F3 only gave a peak at 200 °C (Fig. 6). The peak is so-called *l*-peak due to the physically adsorbed NH_3, probably on Fe_2O_3, which has no acidic properties [28]. This result indicates that [Fe]-SSZ-24 does not have acidity which can be estimated by NH_3-TPD. That is, Fe^{3+} incorporated in the framework of [Fe]-SSZ-24 has much weaker acidity than Al^{3+} of [Al]-SSZ-24 previously reported [10,25].

The overall results for the preparation of [Fe]-SSZ-24 by isomorphous substitution can summarized as follows: [B]-SSZ-24 afforded [Fe]-SSZ-24 by isomorphous substitution with ferric nitrate. However, the hydrolysis of ferric cation inevitably accompanies the formation of ferric hydroxide, which gave Fe_2O_3 after

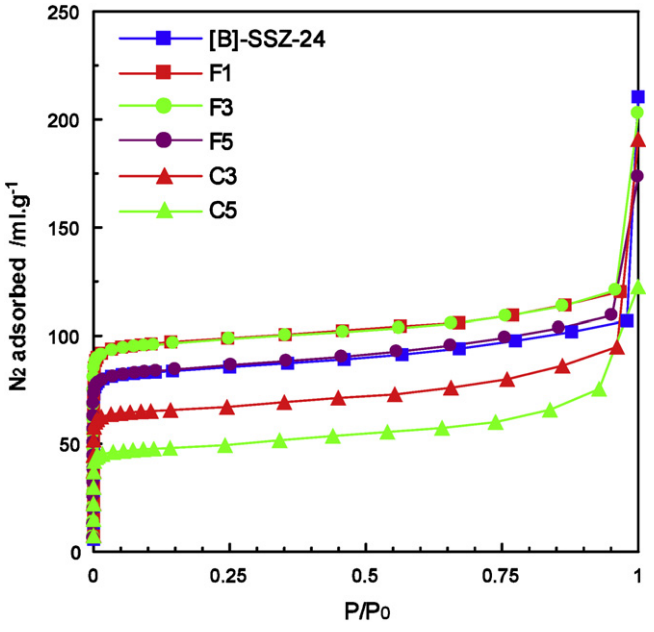

Fig. 4. N_2 adsorption isotherm of [Fe]-SSZ-24.

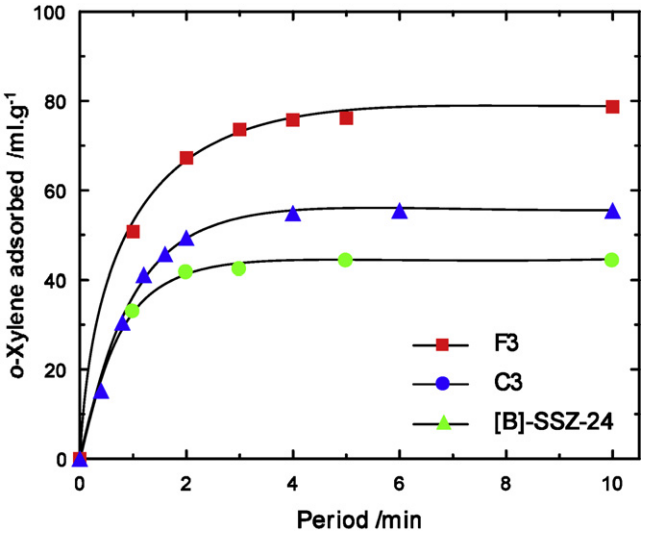

Fig. 5. *o*-Xylene adsorption of [Fe]-SSZ-24.

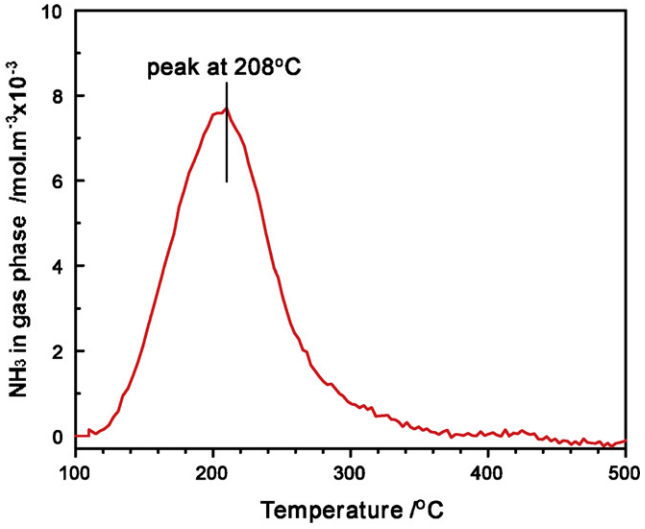

Fig. 6. NH_3-TPD profile of [Fe]-SSZ-24 (F3). Temperature-programmed rate: 10 °C/min.

calcination during the isomorphous substitution. The formation of the hydroxide occurs independently from the zeolites or at the extra-framework site on the internal and external surfaces of the zeolites. Actually, Fe_2O_3/SiO_2 ratios of [Fe]-SSZ-24 shown in Fig. 1 are in the higher levels as B_2O_3/SiO_2 ratio of [B]-SSZ-24. These results suggest that ferric hydroxide is formed during the substitution. The optimization of the ratio of $Fe(NO_3)_3{\cdot}9H_2O$ to [B]-SSZ-24 is important for minimization of the formation of ferric hydroxide and for maximization of Fe^{3+} species in the framework. However, it is difficult to evaluate the amount of Fe^{3+} in the framework in all of the iron species of [Fe]-SSZ-24. From these consideration, the isomorphous substitution in this study was carried out at 0.5 of $Fe(NO_3)_3{\cdot}9H_2O$/[B]-SSZ-24 ratio although some of Fe_2O_3 was accompanied. We examine the isopropylation of BP over [Fe]-SSZ-24 to confirm the formation of Fe^{3+} in the framework of [Fe]-SSZ-24 and to evaluate the acid properties and effectiveness for shape-selective catalysis in the channels of the [Fe]-SSZ-24.

3.2. Isopropylation of BP over [Fe]-SSZ-24

Fig. 7 shows the influence of reaction temperature on the yield of the isopropylated products in the isopropylation of BP over F1, F3, and F5 (SiO_2/Fe_2O_3 = 55, 38, and 28). [B]-SSZ-24 and Fe_2O_3 prepared from the precipitated ferric hydroxide by the calcination at 550 °C had no activities for the isopropylation of BP at 250 °C. On the other hands, [Fe]-SSZ-24 enhanced effectively the catalytic activity for the isopropylation of BP. F1, F3, and F5 had high activities and gave IPBP, DIPB, and triisopropylbiphenyl (TriIPB) isomers, although the catalytic activities were much less than those of [Al-SSZ-24 previously reported [10,15]. Furthermore, the activities of [Fe]-SSZ-24 increased with decreasing the SiO_2/Fe_2O_3 ratio, which means that acid mounts increase by the substitution. These activities also show that [Fe]-SSZ-24 works as an acid catalyst even though its acidity was not observed by NH_3-TPD and that the weak acid sites, due to Fe^{3+} incorporated to the SSZ-24 frameworks, work for the catalyst in the isopropylation of BP. These results mean that the isopropylation of BP occurred solely on [Fe]-SSZ-24, and not on iron species at the extra-framework. However, the activities of F1, F3, and F5 are much lower than those of the [Al]-SSZ-24 catalysts described previously [10,15]: these results are due to the differences in acidity for Al and Fe in the frameworks.

The effects of the reaction temperature and of the SiO_2/Fe_2O_3 ratio of [Fe]-SSZ-24 on the selectivities for DIPB isomers are shown in Fig. 8. The selectivities for 4,4′-DIPB were maintained around 75% at moderate temperatures (250–300 °C) for all [Fe]-SSZ-24; however, they decreased at higher temperatures (325–350 °C), accompanying an increase in the selectivities for 3,4′-DIPB. The decrease in the selectivity for 4,4′-DIPB started at low temperatures for the [Fe]-SSZ-24 sample with a low SiO_2/Fe_2O_3 ratio. Thus, the increase in acid sites on the catalyst enhanced the isomerization of 4,4′-DIPB to 3,4′-DIPB. On the other hands, the selectivities for 4,4′-DIPB in encapsulated products were almost constant at 75%, irrespective of the SiO_2/Fe_2O_3 ratio. These results mean that the acid sites in the channels of [Fe]-SSZ-24 were not active for the isomerization of 4,4′-DIPB and that the isomerization occurred probably on the external acid sites on the [Fe]-SSZ-24 catalyst, as proposed in previous papers for MOR [3,5,8,10].

Fig. 9 shows the amount of coke formation on [Fe]-SSZ-24 during in the isopropylation of BP. It was found to be at a level of 5–9 wt.%, irrespective of the SiO_2/Fe_2O_3 ratio. Coke formation occurred on the internal and external acid sites of [Fe]-SSZ-24.

Highly selective formation of 4,4′-DIPB shows that catalysis occurred in the [Fe]-SSZ-24 channels because of their shape-selective nature and that the isomorphous substitution with ferric nitrate incorporated the formation of a framework Fe^{3+} species of the [Fe]-SSZ-24.

Fig. 10 shows the effects of the SiO_2/Fe_2O_3 ratio on the selectivities for DIPB isomers in the isopropylation of BP at 250 °C and 300 °C. Here, the selectivities for 4,4′-DIPB were around 80% for all

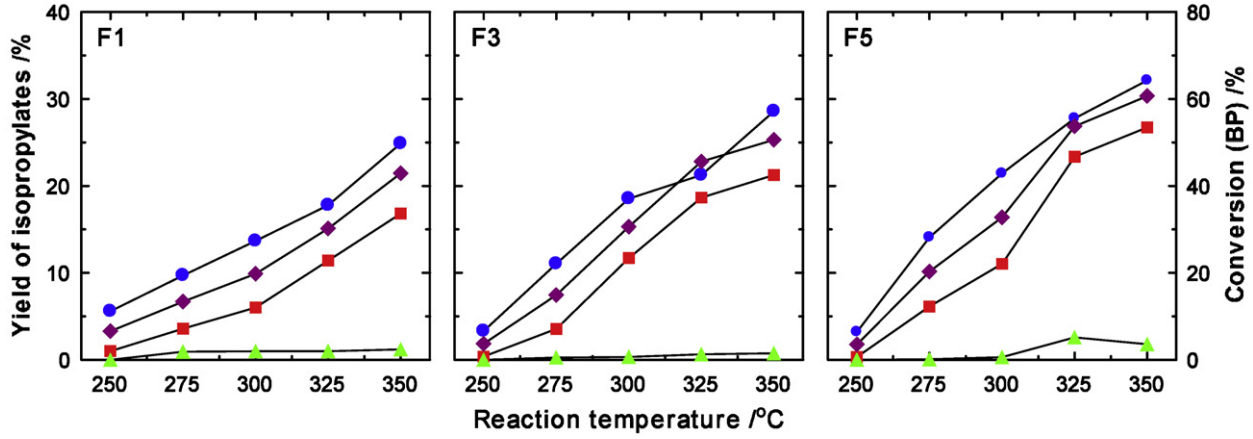

Fig. 7. Effects of reaction temperature on the isopropylation of BP over [Fe]-SSZ-24. Reaction conditions: BP, 3.9 g (25 mmol); catalyst, 0.125 g; temperature, 200–350 °C; propene pressure, 0.8 MPa; period, 4 h. Legends: (♦) conversion (BP); (■) IPBP; (●) DIPB; (▲) triIPB.

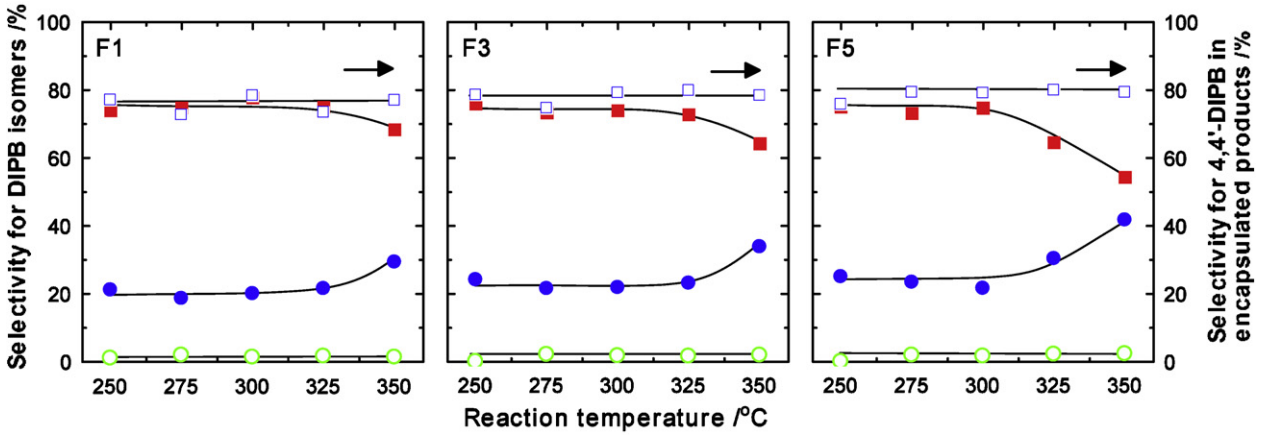

Fig. 8. Effects of reaction temperature on the selectivity for DIPB isomers in the isopropylation of BP over [Fe]-SSZ-24. Reaction conditions: see Fig. 7. Legends: (■) 4,4′-DIPB in bulk products; (□) 4,4′-DIPB in encapsulated products; (●) 3,4′-DIPB; (○) 3,3′-DIPB.

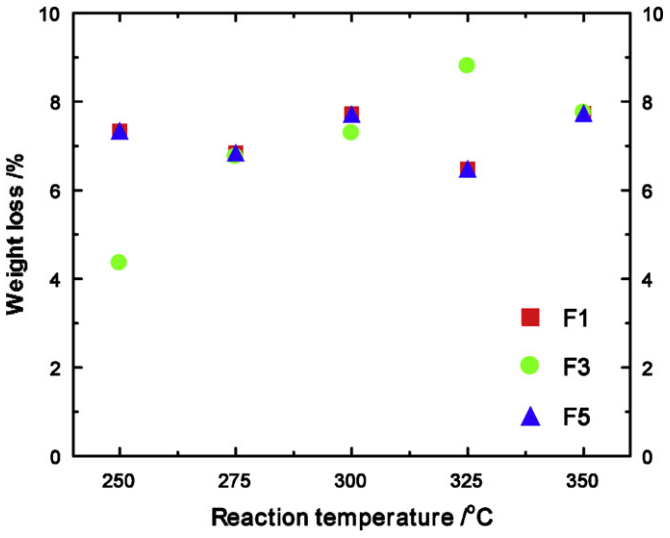

Fig. 9. Effects of reaction temperature on coke formation on [Fe]-SSZ-24 during the isopropylation of BP. Reaction conditions: see Fig. 6.

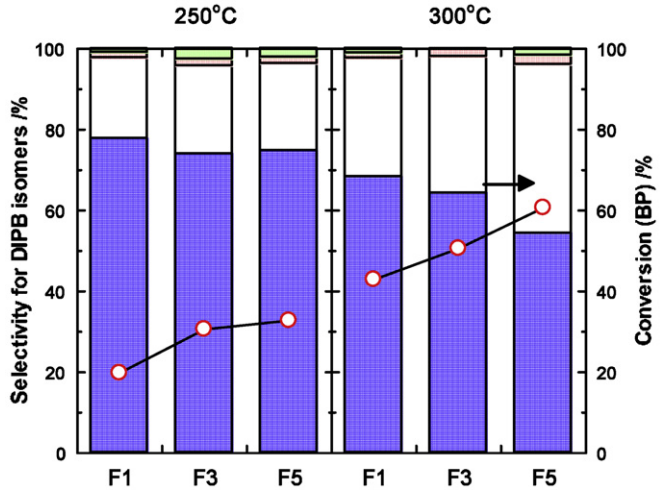

Fig. 10. Effects of the SiO_2/Fe_2O_3 ratio of [Fe]-SSZ-24 on the selectivities for DIPB isomers at 250 and 300 °C in the isopropylation of BP. Reaction conditions: see Fig. 7. Legends: (○) conversion. (■) 4,4′DIPB; (□) 3,4-DIPB; (■) 3,3′-DIPB; (□) 2,*x*-DIPB. (For interpretation of the references to color in this figure legend, the reader is referred to the web version of the article.)

[Fe]-SSZ-24 catalysts (F1, F2 and F3); however, the selectivities for 4,4′-DIPB at 300 °C decreased with the decrease in the ratio. The increase in acidity by the isomorphous substitution resulted in the decrease in the selectivity for 4,4′-DIPB.

Catalytic features of [Fe]-SSZ-24 in the isopropylation of BP clearly indicate that the catalysis occurred on the acid sites appeared on Fe^{3+} incorporated in the frameworks of [Fe]-SSZ-24, where iron species at the extra-frameworks formed from ferric hydroxide during the substitution with ferric nitrate have no influences on the catalytic activities of [Fe]-SSZ-24, and that the weak acid sites of [Fe]-SSZ-24 worked as a catalyst for the isopropylation of BP although the NH_3-TPD indicate no strong acidities on [Fe]-SSZ-24.

3.3. *Shape-selective catalysis over LPMS with AFI topology*

Catalytic performances of LPMS for shape-selective catalysis are generally varied with many factors. Some typical factors are pore structure, physical properties, such as crystal size, morphology, and acidity, type of components, and the distribution of active species, which are also influenced by preparation and post-synthesis methods. Reaction conditions, such as temperature, pressure, period, and catalyst amount, can also influence catalytic performances. However, pore structure is the most important factor in controlling the shape-selectivity of the catalysis. Particularly, the differences in selectivity for 4,4′-DIPB reflect the pore structures of the corresponding zeolites.

Shape-selective catalysis is highly dependent on the confined structure of the zeolites, including the size and shape of the pore entrances and channels. We previously proposed that shape-selective alkylation of BP over MOR occurred inside straight channels [3,5,8]. These results mean that the least bulky isomers with the transition states, that could fit in the MOR channels, only appeared as products. In other words, isopropylation of BP allows for the formation of 4-IPBP from BP and 4,4′-DIPB from 4-IPBP by the steric restriction of the transition states in the MOR channels. These features suggest that shape-selective catalysis selectively occurs to yield the least bulky molecule if pore environments exclude the transition sates of bulky isomers. However, the formation of other bulky isomers can also allow inside the zeolite if the pore environment is large enough for the formation of the transition state to bulky DIPB isomers. Thus, the steric interactions of the isomers with the channels differentiate the transition states during the formation of DIPB isomers in the isopropylation of BP over

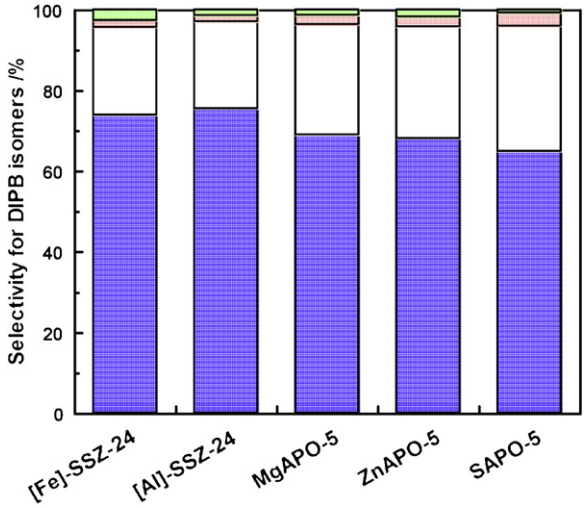

Fig. 11. Selectivities for 4,4′-DIPB in the isopropylation of BP over LPMS with AFI topology. Reaction conditions: see Refs. [15,18–20]. Legend: see Fig. 10.

MOR, which results in the enhancement of selective formation of the slimmest 4,4′-DIPB.

Fig. 11 summarizes the selectivities for the DIPB isomers in the isopropylation of BP over LPMS with AFI topology, where the values of the selectivities were the highest selectivities for 4,4′-DIPB [10,15,18–20,25]. As shown in Fig. 11, the selectivities for 4,4′-DIPB were almost at the same level as 65–75% for all the LPMS, [Fe]-SSZ-24, [Al]-SSZ-24 [10,15,25], MgAPO-5 [18], ZnAPO-5 [19], and SAPO-5 [20] with AFI topology, which commonly have straight channels with 0.72 × 0.72-nm pore entrances. These results of the selectivity for 4,4′-DIPB of the LPMS indicate that their confined structures control the catalysis by their steric restriction of the transition states to form the least bulky 4,4′-DIPB from the other isomers. The results shown in Fig. 11 suggest that the acidities of the LPMS are not principal factors for controlling shape-selective catalysis because these materials had quite different acid strengths and amounts.

The selectivities for 4,4′-DIPB over LPMS with AFI topology were slightly lower than that over MOR (65–75% for AFI and 80–90% for MOR). The differences of the selectivities are due to the difference of their pore structures. MOR channels strictly differentiate the transition state of bulkier 3,4′-DIPB from that of 4,4′-DIPB because MOR has a slightly bigger channels than LPMS with AFI topology.

As discussed above, the decreases in the selectivities for 4,4′-DIPB were observed in the isopropylation of BP over [Fe]-SSZ-24 at high temperatures (325–350 °C). However, the selectivities for 4,4′-DIPB in encapsulated products remained constant even at 350 °C for all of the [Fe]-SSZ-24. These results mean that the [Fe]-SSZ-24 channels can prevent the isomerization of 4,4′-DIPB and that the isomerization of 4,4′-DIPB occurs at external acid sites. Similar prevention of isomerization of 4,4′-DIPB was observed for MOR [3,5,8]. However, we also previously described that the isomerization of 4,4′-DIPB occurred at both the acid sites in internal and external sites in the isopropylation of BP over [Al]-SSZ-24 and SAPO-5 [8,10,20]. The main differences are the acidic properties of these LPMS with AFI topology because [Fe]-SSZ-24 has only weak acid sites in their channels compared to the others.

4. Conclusion

A ferrosilicate, [Fe]-SSZ-24, with AFI topology was prepared from [B]-SSZ-24 by isomorphous substitution with iron, and applied for the isopropylation of biphenyl (BP). The substitution enhanced the activity for the catalysis. Shape-selective formation of 4,4′-diisopropylbiphenyl (4,4′-DIPB) occurred at moderate temperatures (250–300 °C); however, the decrease in the selectivity for 4,4′-DIPB was observed at high temperatures (325–350 °C). The selectivity for 4,4′-DIPB in the encapsulated DIPB isomers was almost constant at all temperatures, irrespective of the SiO_2/Fe_2O_3 ratio. These results mean that the AFI channels have a high potential for discrimination of 4,4′-DIPB from the other possible DIPB isomers at their transition states, and that the channels of [Fe]-SSZ-24 prevent the isomerization of 4,4′-DIPB, although the isomerization occurred at external acids sites at higher temperatures.

LPMS with AFI topology, [Fe]-SSZ-24, [Al]-SSZ-24, MgAPO-5, ZnAPO-5, and SAPO-5, gave similar levels of the selectivity for 4,4′-DIPB in the isopropylation of BP. These results indicate that the framework of the materials primarily governs shape-selective catalysis in the isopropylation of BP; however, their activities are due to their Fe^{3+} incorporated acidic sites.

The results discussed in the paper proved that the isomorphous substitution of [B]-SSZ-24 with iron successfully incorporated with the frameworks of [Fe]-SSZ-24; however, the formation of Fe_2O_3 cannot be prevented completely on the internal and external surfaces of the zeolites or independently from the zeolites. The catalytic features of [Fe]-SSZ-24 in the isopropylation of BP clearly show that the catalysis occurred on acid sites appeared from Fe^{3+} incorporated to the framework, where iron species at the extra-frameworks formed from ferric hydroxide during the substitution with ferric nitrate have no influences on catalytic properties of [Fe]-SSZ-24. Furthermore, investigations are now underway to establish an effective isomorphous substitution of boron to Fe^{3+} species in the framework of the zeolites for the development of catalysts with high performance.

Acknowledgements

A part of this work was financially supported by Grant-in-Aids for Scientific Research ((B) 16310056, (B) 19310060, and (C) 21510098)), the Japan Society for the Promotion of Science (JSPS). Y.S. would also like to thank Dr. Ajayan Vinu of the National Institute of Materials Science (NIMS) for his helpful discussion and the Department of Research, Nagoya Industrial Science Research Institute for their continuing cooperation.

Appendix A. Supplementary data

Supplementary data associated with this article can be found, in the online version, at doi:10.1016/j.molcata.2011.08.027.

References

[1] S.M. Csicsery, Zeolites 4 (1984) 202.
[2] P.B. Venuto, Micropor. Mater. 2 (1994) 297.
[3] Y. Sugi, Y. Kubota, in: J.J. Spivey (Ed.), Catalysis, Specialist Periodical Report, vol. 13, Royal Soc. Chem., 1997, pp. 55–84 (Chapter 3).
[4] Y. Sugi, J. Chin. Chem. Soc. 57 (2010) 1.
[5] Y. Sugi, J. Jpn. Petrol. Inst. 53 (2010) 263.
[6] T. Matsuzaki, Y. Sugi, T. Hanaoka, K. Takeuchi, H. Arakawa, T. Tokoro, G. Takeuchi, Chem. Express 4 (1989) 413.
[7] G.S. Lee, J.J. Maj, S.C. Rocke, J.M. Garces, Catal. Lett. 2 (1989) 243.
[8] Y. Sugi, S. Tawada, T. Sugimura, Y. Kubota, T. Hanaoka, T. Matsuzaki, K. Nakajima, K. Kunimori, Appl. Catal. A: Gen. 189 (1999) 251.
[9] R.K. Ahedi, S. Tawada, Y. Kubota, Y. Sugi, J.H. Kim, J. Mol. Catal. A: Chem. 197 (2003) 133.
[10] A. Ito, H. Maekawa, H. Kawagoe, K. Komura, Y. Kubota, Y. Sugi, Bull. Chem. Soc. Jpn. 80 (2007) 215.
[11] H. Maekawa, A. Iida, C. Naitoh, K. Nakagawa, K. Komura, Y. Kubota, Y. Sugi, D.-H. Choi, J.-H. Kim, G. Seo, J. Mol. Catal. A: Chem. 274 (2007) 24.
[12] T. Shibata, S. Suzuki, H. Kawagoe, K. Komura, Y. Kubota, Y. Sugi, J.-H. Kim, G. Seo, Micropor. Mesopor. Mater. 116 (2008) 216.
[13] H. Maekawa, T. Shibata, A. Niimi, C. Asaoka, K. Yamasaki, H. Naiki, K. Komura, Y. Kubota, Y. Sugi, J.-Y. Lee, J.-H. Kim, G. Seo, J. Mol. Catal. A: Chem. 279 (2008) 27.

[14] H. Naiki, K. Komura, J.-H. Kim, G. Seo, Y. Sugi, Micropor. Mesopor. Mater. 143 (2011) 383.
[15] Y. Sugi, H. Maekawa, A. Ito, C. Ozawa, T. Shibata, A. Niimi, C. Asaoka, K. Komura, Y. Kubota, J.-Y. Lee, J.-H. Kim, G. Seo, Bull. Chem. Soc. Jpn. 80 (2007) 2232.
[16] Y. Sugi, H. Maekawa, S.A.R. Mulla, A. Ito, C. Naitoh, K. Nakagawa, K. Komura, Y. Kubota, J.-H. Kim, G. Seo, Bull. Chem. Soc. Jpn. 80 (2007) 1418.
[17] Y. Sugi, H. Maekawa, Y. Hasegawa, A. Ito, R. Asai, D. Yamamoto, K. Komura, Y. Kubota, J.-H. Kim, G. Seo, Catal. Today 131 (2008) 413.
[18] H. Maekawa, S.K. Saha, S.A.R. Mulla, S.B. Waghmode, K. Komura, Y. Kubota, Y. Sugi, J. Mol. Catal. A: Chem. 263 (2007) 238.
[19] S.K. Saha, H. Maekawa, S.B. Waghmode, S.A.R. Mulla, K. Komura, Y. Kubota, Y. Sugi, S.-J. Cho, Mater. Trans. 46 (2005) 2659.
[20] M. Bandyopadhyay, R. Bandyopadhyay, S. Tawada, Y. Kubota, Y. Sugi, Appl. Catal. A: Gen. 225 (2002) 51.
[21] Ch. Baerlocher, L.B. McMusker, D.H. Olson, Atlas of Zeolite Framework Types, 6th ed., Elsevier, Amsterdam, 2007, http://www.iza-structure.org/databases/.
[22] S.I. Zones, U.S. Patent 4,665,110 (1987).
[23] S.I. Zones, Y. Nakagawa, Micropor. Mater. 2 (1994) 557.
[24] R.F. Lobo, M.E. Davis, Micropor. Mater. 3 (1994) 61.
[25] Y. Kubota, H. Maekawa, S. Miyata, T. Tatsumi, Y. Sugi, Micropor. Mesopor. Mater. 101 (2007) 115.
[26] C.F. Bases Jr., R.E. Mesner, The Hydrolysis of Cations, John Wiley & Sons, Inc., New York, 1976.
[27] R.L. Blake, R.E. Hessevick, T. Zoltai, L.W. Finger, Am. Mineral. 51 (1966) 123.
[28] M. Niwa, N. Katada, Catal. Surv. Jpn. 1 (1997) 215.